Direct Synthesis of MgH_2 Nanofibers at Different Hydrogen Pressures

Chunyu Zhu[a], Haruya Hayashi[a], Itoko Saita[b], Tomohiro Akiyama[a *]

[a] *Center for Advanced Research of Energy Conversion Materials, Hokkaido University, Sapporo 060-8628, Japan*

[b] *Energy Technology Research Institute, National Institute of Advanced Industrial Science and Technology, Ibaraki 305-8565, Japan*

Corresponding author: Tel.: +81-11-706-6842; Fax: +81-11-726-0731.

E-mail address: takiyama@eng.hokudai.ac.jp (Tomohiro Akiyama)

ABSTRACT:

This paper describes the direct synthesis of magnesium hydride (MgH_2) nanofibers by hydriding chemical vapor deposition (HCVD), in which the effect of hydrogen pressure on the production rate, the composition and the shape of products obtained were examined by using X-ray diffraction (XRD), scanning electron microscopy (SEM) and Brunauer-Emmett-Teller (BET). The XRD patterns showed that the main product in each case was MgH_2; in particular, the products formed at 2, 3 and 4 MPa were highly pure. In contrast, at a hydrogen pressure of 1 MPa, unhydrided Mg was deposited along with MgH_2. The SEM images also revealed orientation of the as-deposited products; higher pressures of 3 and 4 MPa caused the formation of straight and curved nanofibers, and lower ones of 1 and 2 MPa, highly curved nanofibers and nanorods with a few straight nanofibers. With pressurizing hydrogen, not only the BET specific surface areas of the products but also the production rate increased. The results also appealed that HCVD could control the shape/size of MgH_2 nanofibers by changing the pressure via only a single operation.

Keywords: Hydrogen Storage; Magnesium Hydride; Nanofiber; Hydriding Chemical Vapor Deposition

1. Introduction

Crystal growth of nano materials has received increased attention because of their unique properties. Historically, Dr. Ukichiro Nakaya [1] of Hokkaido University, Sapporo, is world famous because of elucidating the relationship between the shapes of snow crystals and the atmospheric conditions, i.e. the temperature and the supersaturation of the atmosphere. In this respect, the synthesis of magnesium nano materials under different conditions could be of interest in the field of hydrogen storage. Magnesium hydride (MgH_2), which contains 7.6 mass% of hydrogen, is a promising candidate for hydrogen storage applications because of its relative abundance, light weight and high hydrogen content [2-4]. However, the high operation temperature of 300 °C in equilibrium pressure of 0.1 MPa, slow hydrogen adsorption kinetics of bulk Mg, and its easy poisoning by air/oxygen have limited its applications [2, 3].

Two promising approaches have been proposed to overcome these drawbacks. In one approach, Mg-rich alloys and compounds are tailored for various applications, and in the other, the particle size of Mg is reduced to the order of a few microns or nanometers. *Hydriding Combustion Synthesis* (HCS) using exothermic reaction among particles and hydrogen at high hydrogen pressure was first proposed for producing Mg-based hydride; however, the resulting alloys suffered from small hydrogen storage capacity. For example, Mg_2NiH_4 produced by HCS has been studied extensively because of its excellent hydrogenation kinetics, but thermodynamically it still requires 280 °C for 0.1 MPa H_2; furthermore, its low hydrogen absorption capacity of 3.6 mass% has hampered its development and widespread use [5, 6]. Reactive ball milling (mechanical alloying) of

Mg/MgH_2 with suitable elements, alloys, or compounds is one of the most important methods used for producing micron-sized Mg-based metal hydride powders with nanometer-sized grains [7-10]. However, this method is only suitable for the laboratory-scale production of such alloys and is energy- & time-consuming in general. With the milling technique, the particle size of Mg hydrides can be reduced to 300 nm [10], while grain sizes can be reduced to 10－50 nm [10, 11].

The mechanism underlying the hydrogenation of Mg has not been fully understood yet, and hydrogen desorption restricts the use of Mg as a practical hydrogen storage material. Basically, hydrogenation of bulk Mg, expressed as a gas－solid reaction: $H_2(g) + Mg(s) \rightarrow MgH_2(s)$, involves three major steps: hydrogen dissociation, hydrogen diffusion, and MgH_2 formation. Each of these steps can influence the other two steps and make the overall hydrogenation process increasingly complex [4]. Further, the hydrogen diffusion in bulk Mg is slow enough to be the rate-determining step in the conventional gas－solid reaction [12].

The maximum purity of commercially available MgH_2 is 98% (products from Alfa Aesar and Sigma Aldrich). The activation barrier of MgH_2 makes it unfit for the practical use as a hydrogen storage material or as a starting material for the synthesis of other hydrogen storage materials. However, MgH_2 has been used as the starting chemical with an amide to produce lightweight metal-based hydrogen storage materials [13-15]. MgH_2 can also be used in portable fuel cells, wherein it undergoes hydrolysis with pure water to produce 15.2 mass% of hydrogen [16, 17]. Another example of the mobile application for MgH_2 is that it is used as a negative electrode in Li-ion batteries; the MgH_2 electrode shows advantages of having a high, reversible capacity of 1480 $mAhg^{-1}$ at an average

voltage of 0.5 V versus $Li^+/Li°$ which is suitable for a negative electrode [18]. However, the currently available MgH_2 products often contain a large amount of unhydrided Mg or are poisoned by air/oxygen. Thereby, there is an urgent need to develop a method for synthesizing high-purity MgH_2.

Hydriding Chemical Vapor Deposition (HCVD), which is used to synthesize metal hydrides in the gas phase, is expected to be a solution to the aforementioned problems [19]. The rate-determining step of hydrogen diffusion in bulk Mg is absolutely eliminated when MgH_2 is synthesized under a high-pressure hydrogen atmosphere and vaporized Mg, as expressed by the gas—gas reaction: $H_2(g) + Mg(g) \rightarrow MgH_2(s)$. High-purity single crystals of MgH_2 in the shape of nanofibers are obtained by this newly introduced HCVD method. The hydrogen sorption rate of the obtained MgH_2 nanofibers is much greater than that of bulk Mg; this is due to the short reaction pathway along the radial direction of the fibers [19, 20].

All of the previous studies were carried out at a fixed hydrogen pressure of 4.0 MPa for analyzing the feasibility of synthesizing MgH_2 and for confirming its microstructure. The two series reactions of $Mg(s) \rightarrow Mg(g)$ and $Mg(g) + H_2(g) \rightarrow MgH_2(s)$ are obviously pressure dependent. However, there is no information on pressure dependence although such information is important from the viewpoints of reaction kinetics, crystallography and nanotechnology. Therefore, the purpose of this study is to study the direct synthesis of MgH_2 nanofibers at different hydrogen pressures, in which the effect of hydrogen pressure on HCVDed MgH_2 is mainly investigated via X-ray diffraction (XRD), scanning electron microscopy (SEM) and Brunauer-Emmett-Teller (BET) measurement.

2. Experimental Section

2.1. Specification of the reactor

Fig. 1 shows the schematic diagram of the reactor furnace used in this study [21]. An Inconel tube with an inside length of 520 mm and inner diameter of 70 mm was used as the reactor. The maximum setting temperature and maximum atmospheric pressure inside the furnace were 600 ^{o}C and 6.0 MPa, respectively. The samples were placed at the center of the reactor tube by using a sample frame and a stainless steel sample container. The hydrogen pressure measured by a pressure gauge was fed back to the control system with an accuracy of ±0.015 MPa.

2.2. Preparation and characterization of the samples

The MgH_2 samples were prepared from commercially available Mg (purity 99.9%, particle size < 75 μm) and highly pure H_2 (99.99999%). Ten grams of the Mg raw material was placed in the sample container without any pre-treatment. The container was fixed onto the sample frame by matching the three holes on the bottom of the container to the three thermocouples, as shown in Fig. 1. The samples were vaporized by heating at 600 ^{o}C for 20 h and allowed to cool naturally under hydrogen pressures of 1, 2, 3 and 4 MPa. The reactants of H_2 and Mg vapor were deposited on the cooled Inconel flange, whose temperature was measured to be around 400 °C. Before heating, the furnace was

evacuated to 10 Pa using a rotary pump, filled with 0.1 MPa of argon, and re-evacuated. This procedure was repeated twice for the removal of air/oxygen from the system.

The as-prepared samples were characterized by powder X-ray diffraction (XRD, Rigaku Miniflex, CuKα), scanning electron microscopy (SEM, JEOL, JSM-7400F) and Brunauer-Emmett-Teller (BET, Yuasa Ionics, Autosorb 6AG) nitrogen adsorption－desorption measurements.

3. Results and Discussion

3.1. Effect of hydrogen pressure on the production rate and purity of MgH_2

The products deposited on the cooled substrate were collected using a sheet of paper in a manner described elsewhere [19]. The observed thickness, δ, of the sheet layers of the products, which were formed at different hydrogen pressures, deposited on the flange (see Fig. 2-(a) and Fig. 3-(a)) is as follows:

(1) At 1 MPa (sample A): δ < 0.50 mm (could not be collected in the form of a complete sheet);

(2) At 2 MPa (sample B): δ < 1.00 mm (mostly in the range of 0.50~1.00 mm);

(3) At 3 MPa (sample C): δ < 2.00 mm (mostly in the range of 1.00~2.00 mm);

(4) At 4 MPa (sample D): δ < 4.00 mm (mostly in the range of 2.00~3.00 mm);

Consequently, the production rate (amount of products) increased with the hydrogen pressure, as could be demonstrated from the reaction equilibrium of the dissociation of MgH_2. Fig. 4 shows the dissociation pressure of MgH_2 as a function of temperature (calculated using HSC Chemistry, version 5.1)

$$MgH_2(s) \leftrightarrow Mg(s) + H_2(g) \qquad (1)$$

The pressure quotient, J_p, of this reaction is defined as

$$J_p = P_{H_2} \big/ P^o \qquad (2)$$

where P_{H_2} is the ambient hydrogen pressure, and P^o is the equilibrium pressure at a certain temperature. The deposition temperature in our experiment is maintained constant at 400 °C; further, $P_{H_2(D)} > P_{H_2(C)} > P_{H_2(B)} > P_{H_2(A)} \approx P^o$, and hence, $J_{p(D)} > J_{p(C)} > J_{p(B)} > J_{p(A)} \approx K°$ ($K°$ is the equilibrium constant at 400 °C). Therefore, we conclude that at high hydrogen pressures such as 3 and 4 MPa, which are denoted by areas C and D in Fig. 4, there is a large driving force for the formation of a large amount of MgH_2; this is due to being far away from the dissociation area.

Fig. 2-(b) shows the images of the samples prepared for XRD analysis along with the image of the commercially available product (Alfa Aesar) for comparison. These images reveal that the products synthesized at hydrogen pressures of more than 2 MPa are snow-white in color, indicating the high purity of MgH_2 produced in these cases (as confirmed by the XRD analysis in the following part). However, the product obtained at a hydrogen pressure of 1 MPa is gray in color, similar to the Alfa Aesar product.

Fig. 5 shows the XRD patterns of the products prepared at different hydrogen pressures, as well as those of the Alfa Aesar product. From this figure, apparently, all the peaks corresponding to the products synthesized at pressures of 2, 3 and 4 MPa can be indexed to a single phase of the tetragonal rutile-type structure of β-MgH_2. However, the sample prepared at a hydrogen pressure of 1 MPa contains metallic Mg as impurity owing to the dissociation of MgH_2 near the equilibrium area (see area A in Fig. 4). Peaks corresponding to MgO appear in the XRD patterns of the product obtained at 1 MPa; MgO is regarded to be formed at the exposure of this product to air. In contrast, the Alfa

Aesar product contains a large amount of unhydrided Mg and detectable amounts of $Mg(OH)_2$ as impurity.

Very interestingly, we observed a silver-gray material deposited along with the snow-white product on the flange at 1 MPa in our experiments. We separated this material and analyzed it by XRD; the results reveal that it is pure Mg (Fig. 6). The XRD patterns also reveal that the as-deposited Mg has a hexagonal close-packed crystal structure with a distinct (002) preferred orientation. The lattice constants determined from the XRD patterns are $a \approx 0.3228$ nm and $c \approx 0.5240$ nm; these values are slightly larger than the standard values obtained for the Mg raw material having $a_o = 0.3223$nm and $c_o = 0.5232$ nm.

The abovementioned silver-gray material was used for SEM observations (Fig. 7). The SEM images reveal that Mg has dendritic or hexagonal plate shapes, similar to the vapor-deposited Mg formed in the Pidgeon process [22]. The formation mechanism of Mg crystals will be discussed latter.

3.2. Structural analysis and growth mechanism of MgH_2 nanofibers

Fig. 8 shows the SEM images of the as-deposited products. The samples were collected from the same position on the flange and stored in an argon atmosphere until investigation. The results of the SEM analysis are summarized as follows:

(1). At 4 MPa (sample D): Straight, needle-like, rod-like, and curved nanofibers are formed. These fibers have diameters of 100~1000 nm, with most of them in the range of 300~500 nm. Fibers with diameters less than 500 nm can grow to a length of several tens

of microns. However, fibers with diameters greater than 800 nm tend to be curved but short.

(2). At 3 MPa (sample C): Straight, needle-like, rod-like, curved and somewhat root-like nanofibers are formed. These fibers also have diameters in the range of 100~1000 nm; and most of them are thinner than 500 nm. Fibers with diameters of less than 500 nm can grow to a length of several tens of microns. Fibers that are thicker than 800 nm tend to be curved but short; some with diameters greater than 1000 nm have a root-like appearance.

(3). At 2 MPa (sample B): Curved nanofibers, nanorods, and root-like MgH_2 with a few straight nanofibers are formed. Though these fibers have diameters in the range of 100~1000 nm, they are not as long as those formed at 3 and 4 MPa. Furthermore, the root-like and curved nanofibers are thicker than 2000 nm, and some of them tend to become agglomerates.

(4). At 1 MPa (sample A): Highly curved and root-like nanofibers grow from agglomerates of MgH_2 with a few straight nanofibers. The fibers are very short and are as thin as those obtained in the previous three cases.

In summary, at higher hydrogen pressures of 3 and 4 MPa, the products grow in a more uniform manner (fiber-like, straight or curved; longer and thinner). In contrast, at lower hydrogen pressures of 1 and 2 MPa, the products grow much thicker and are disorderly, and even become agglomerates under 1 MPa. The typical morphology of the aforementioned products is proposed in Fig. 9 as well as the relationship between the production rate and hydrogen pressure. The Brunauer-Emmett-Teller (BET) nitrogen

adsorption-desorption analysis shows that the specific surface areas of the samples A, B, C and D are $\approx$ 6.2, 8.9, 11.5 and 14.1 m^2/g, respectively (as shown in Fig. 3-(b)).

Transmission electron microscopy (TEM) measurements reveal that the abovementioned nanofibers are single crystals of MgH_2 in our previous study [19]. The results of this study show that the purity and morphology of nanofiber-like MgH_2 is quite dependent on hydrogen pressure. However the growth mechanism is still unclear.

One-dimensional nanostructures, such as semiconductor nanowires [23, 24] and metallic nanowires [25, 26], have aroused tremendous interest because of their novel properties and potential applications in areas such as electronic devices, optical devices, magnetic devices and nanosensors [27]. Several mechanisms including vapor-liquid-solid (VLS) [23, 28], vapor-solid-solid (VSS) [24, 29] and vapor-solid (VS) [25, 26] have been proposed to explain the growth of nanowires. In VLS and VSS growth, a vapor-phase precursor is catalytically decomposed at a metal nano-particle surface, forming a supersaturated eutectic liquid; the solid crystalline nanowires grow by precipitation from a liquid catalyst in VLS and from a solid catalyst in VSS. Since no catalysts are used in the process of synthesizing MgH_2, the VS mechanism can be used to explain the growth mechanism of MgH_2 nanofibers. For the VS mechanism, the degree of supersaturation at a particular experimental condition benefits the growth of nanowires [25, 26]. Namely, when the degree of supersaturation is maintained below some critical value, nanowires could be fabricated, and above the value bulk crystal or powder is formed. The supersaturation factor was controlled by adjusting the experimental conditions such as temperature and pressure in order to manipulate the lateral dimension of the nanowires.

Mg nanowires and various Mg structures (spheres, flakes, rods and sea-urchinlike) have been successfully prepared by Li et al [30, 31] by using a vapor-transport approach under Ar gas flow. Different shapes of Mg were achieved by changing the evaporation temperature of Mg and Ar flow rate; and they found the as-prepared Mg micro/nanosturtures is strongly influenced by the degree of supersaturation of Mg in the chamber. Zlotea et al [32-34] have synthesized similar single crystals of nanowhiskers (or nanowires, nanofibers) of MgH_2 in the range of nanometers and micrometers by hydrogen-induced disproportionation of bulk $Mg_{24}Y_5$ [33], Mg_5Ga_2 and Mg_6Pd [34]. The VLS model has been proposed to explain the growth mechanism of the MgH_2 nanowhiskers.

The reactions that occurred in the deposition area in our reactor are thought to include the following three:

$$Mg(g) + H_2(g) \leftrightarrow MgH_2(s) \quad (3)$$

$$Mg(g) \leftrightarrow Mg(s) \quad (4)$$

$$Mg(s) + H_2(g) \leftrightarrow MgH_2(s) \quad (5)$$

Reaction (3) expresses the direct formation of MgH_2 fibers from sublimated Mg vapor and hydrogen gas; reaction (4) is the solidification of Mg vapor; and reaction (5) is the hydriding of solidified Mg. It is obvious that the fabrication of MgH_2 nanofibers is dependent both on H_2 pressure and on the Mg vapor supplied. In this case, when the

hydrogen atmospheric pressure is lowered, the solidification of Mg will be enhanced; and if enough Mg vapor is supplied, at a proper deposition temperature (the deposition temperature affects the supersaturation degree of Mg and then controls the shape of the Mg deposited like in the Pidgeon process) the Mg grows into a dendritic crystal (as shown in Fig 7). The results of this study show that high a H_2 pressure will benefit producing uniform and thin MgH_2 naonofibers; however, the growth of the MgH_2 crystal must be also dependent on the Mg vapor supplied, deposition temperature (which controls the shape of the solidified Mg and dissociation of MgH_2); more complex study is needed in the near future to demonstrate such a hypothesis.

MgH_2 was first produced in 1912 via the pyrolysis of ethyl magnesium iodide in vacuum at 175 °C; however, the direct synthesis of this compound from elements of Mg and H_2 was carried out as late as 1951 [35]. This direct synthesis was carried out under a hydrogen pressure of 20 MPa at 500 °C using MgI_2 as the catalyst; however, even under such harsh reaction conditions, the yield of the product was as low as 68%. Dymova et al. could obtain MgH_2 with 97~98% purity by using iodine (0.5~1%) as the catalyst and by carrying out mechanical grinding in a ball mill at 380~450 °C and 10~20 MPa according to [36]. The results of our study show that our newly developed HCVD method is more suitable for the production of high-purity MgH_2 at a relatively low pressure via a simple operation.

4. Conclusions

The feasibility of *Hydriding Chemical Vapor Deposition* (HCVD) of high-purity MgH_2 nanofibers at different pressures was studied. The products were obtained directly from magnesium vapor and hydrogen and were analyzed by XRD, BET and SEM. Hydrogen pressure was a key factor to affect the amount/shape of the pure MgH_2 product. The following conclusions were obtained.

(1) The deposition amount of high-purity MgH_2 increased with increasing pressure in the order of 2, 3 and 4 MPa at a constant temperature of 400 °C. In contrast, a mixture of MgH_2 and unhydrided Mg was obtained at 1 MPa.

(2) Low hydrogen pressures of 1 and 2 MPa formed curved root-like nanofibers or nanorods with a few straight nanofibers, as confirmed by SEM observations. However, the micro-morphology of the as-deposited MgH_2 at high hydrogen pressures of 3 and 4 MPa revealed nanofibers with uniform shapes. These nanofibers had diameters in the range of 100 to 1000 nm and lengths of the order of several tens of microns, and according to the BET measurement specific surface areas increase with increasing the hydrogen pressure.

In conclusion, pressurizing hydrogen in HCVD offers many benefits for minimizing the operation time, improving the purity of the product, and controlling the shape of the MgH_2 nanofibers.

REFERENCES

[1] Nakaya U. Snow Crystals, Natural and Artificial. Cambridge: Harvard Univ. Press; 1954. pp. 510.

[2] Schlapbach L, Zuttel A. Hydrogen-storage materials for mobile applications. Nature 2001;414:353.

[3] Sakintuna B, Lamari-Darkrim F, Hirscher M. Metal hydride materials for solid hydrogen storage: A review. Int J Hydrogen Energy 2007;32:1121.

[4] Yao XD, Lu GQ. Magnesium-based materials for hydrogen storage: Recent advances and future perspectives. Chin Sci Bull 2008;53:2421.

[5] Li LQ, Akiyama T, Yagi J. Production of hydrogen storage alloy of Mg_2NiH_4 by hydriding combustion synthesis in laboratory scale. J Mater Synth Process 2000;8:7.

[6] Akiyama T, Isogai H, Yagi J. Hydriding combustion synthesis for the production of hydrogen storage alloy. J. Alloy. Compd. 1997;252:L1.

[7] Zaluska A, Zaluski L, Strom-Olsen JO. Nanocrystalline magnesium for hydrogen storage. J. Alloy. Compd. 1999;288:217.

[8] Polanski M, Bystrzycki J, Plocinski T. The effect of milling conditions on microstructure and hydrogen absorption/desorption properties of magnesium hydride (MgH_2) without and with Cr_2O_3 nanoparticles. Int J Hydrogen Energy 2008;33:1859.

[9] Recham N, Bhat VV, Kandavel A, Aymard L, Tarascon JM, Rougier A. Reduction of hydrogen desorption temperature of ball-milled MgH_2 by NbF_5 addition. J. Alloy.

Compd. 2008;464:377.

[10] Aguey-Zinsou KF, Fernandez JRA, Klassen T, Bormann R. Effect of Nb_2O_5 on MgH_2 properties during mechanical milling. Int J Hydrogen Energy 2007;32:2400.

[11] Wagemans RWP, van Lenthe JH, de Jongh PE, van Dillen AJ, de Jong KP. Hydrogen storage in magnesium clusters: Quantum chemical study. J. Am. Chem. Soc. 2005;127:16675.

[12] Fernandez JF, Sanchez CR. Rate determining step in the absorption and desorption of hydrogen by magnesium. J. Alloy. Compd. 2002;340:189.

[13] Hu J, Xiong Z, Wu G, Chen P, Murata K, Sakata K. Effects of ball-milling conditions on dehydrogenation of $Mg(NH_2)_2$-MgH_2. J Power Sourc 2006;159:120.

[14] Luo WF. ($LiNH_2$-MgH_2): a viable hydrogen storage system. J. Alloy. Compd. 2004;381:284.

[15] Liu YF, Zhong K, Gao MX, Wang HH, Pan HG, Wang QD. Hydrogen storage in a $LiNH_2$-MgH_2 (1 : 1) system. Chem Mater 2008;20:3521.

[16] Grosjean MH, Zidoune M, Roue L, Huot JY. Hydrogen production via hydrolysis reaction from ball-milled Mg-based materials. Int J Hydrogen Energy 2006;31:109.

[17] Grosjean MH, Zidoune M, Huot JY, Roue L. Hydrogen generation via alcoholysis reaction using ball-milled Mg-based materials. Int J Hydrogen Energy 2006;31:1159.

[18] Oumellal Y, Rougier A, Nazri GA, Tarascon JM, Aymard L. Metal hydrides for lithium-ion batteries. Nat Mater 2008;7:916.

[19] Saita I, Toshima T, Tanda S, Akiyama T. Hydriding chemical vapor deposition of metal hydride nano-fibers. Mater Trans 2006;47:931.

[20] Saita I, Toshima T, Tanda S, Akiyama T. Hydrogen storage property of MgH_2 synthesized by hydriding chemical vapor deposition. J. Alloy. Compd. 2007;446-447:80.

[21] Li L, Saita I, Saito K, Akiyama T. Effect of synthesis temperature on the purity of product in hydriding combustion synthesis of Mg_2NiH_4. J. Alloy. Compd. 2002;345:189.

[22] Magnesium. http://en.wikipedia.org/wiki/Magnesium

[23] Perea DE, Hemesath ER, Schwalbach EJ, Lensch-Falk JL, Voorhees PW, Lauhon LJ. Direct measurement of dopant distribution in an individual vapour-liquid-solid nanowire. Nat Nano 2009;4:315.

[24] Kodambaka S, Tersoff J, Reuter MC, Ross FM. Germanium nanowire growth below the eutectic temperature. Science 2007;316:729.

[25] Hsu Y-J, Lu S-Y. Vapor-Solid Growth of Sn Nanowires: Growth Mechanism and Superconductivity. J Phys Chem B 2005;109:4398.

[26] Wang Q, Chen G, Zhou N. The large-scale synthesis and growth mechanism of II-B metal nanosponges through a vacuum vapor deposition route. Nanotechnology 2009;20:9.

[27] Patolsky F, Weizmann Y, Willner I. Actin-based metallic nanowires as bio-nanotransporters. Nat Mater 2004;3:692.

[28] Wagner R, Ellis W. Vapor-liquid-solid mechanism of single crystal growth. Appl Phys Lett 1964;4:89.

[29] Kamins TI, Williams RS, Basile DP, Hesjedal T, Harris JS. Ti-catalyzed Si nanowires by chemical vapor deposition: Microscopy and growth mechanisms. J. Appl. Phys. 2001;89:1008.

[30] Li WY, Li CS, Ma H, Chen J. Magnesium nanowires: Enhanced kinetics for hydrogen absorption and desorption. J. Am. Chem. Soc. 2007;129:6710.

[31] Li WY, Li CS, Zhou CY, Ma H, Chen J. Metallic magnesium nano/mesoscale structures: Their shape-controlled preparation and Mg/air battery applications. Angew Chem Int Ed 2006;45:6009.

[32] Zlotea C, Sahlberg M, Zbilen S, Moretto P, Andersson Y. Hydrogen desorption studies of the $Mg_{24}Y_5$-H system: Formation of Mg tubes, kinetics and cycling effects. Acta Mater 2008;56:2421.

[33] Zlotea C, Lu J, Andersson Y. Formation of one-dimensional MgH_2 nano-structures by hydrogen induced disproportionation. J. Alloy. Compd. 2006;426:357.

[34] Zlotea C, Andersson Y. Microstructural modifications induced by hydrogen absorption in Mg_5Ga_2 and Mg_6Pd. Acta Mater 2006;54:5559.

[35] Magnesium hydride. http://en.wikipedia.org/wiki/Magnesium_hydride

[36] Klyamkin SN. Metal hydride compositions on the basis of magnesium as materials for hydrogen accumulation. Russ. J. Gen. Chem. 2007;77:712.

Figure captions

Fig. 1 − Schematic diagram of the reactor used for HCVD [21].

Fig. 2 − (a): Images of the as-deposited products formed on the Inconel flange at different H_2 pressures of 1 MPa (A), 2 MPa (B), 3 MPa (C) and 4 MPa (D) (the two holes on the flange are left for holder). (b): As-deposited samples prepared for XRD analysis (A–D); commercially available MgH_2 (R) from Alfa Aesar is shown for comparison.

Fig. 3 − (a): Layer thickness distribution of the as-deposited products on the flange synthesized at hydrogen pressures of 1, 2, 3 and 4 MPa. (b): Specific surface areas of the as-deposited products synthesized at hydrogen pressures of 1, 2, 3 and 4 MPa.

Fig. 4 − Dissociation pressure of MgH_2 vs. temperature (calculated using HSC Chemistry, version 5.1).

Fig. 5 − XRD patterns of the as-deposited products synthesized under H_2 pressures of 1 MPa (A), 2 MPa (B), 3 MPa (C) and 4 MPa (D). XRD patterns of commercially available MgH_2 (R) from Alfa Aesar are shown for comparison. MgH_2 (▼), Mg (□), MgO (●), $Mg(OH)_2$ (○).

Fig. 6 − XRD patterns of the silver-gray material separated from the as-deposited product obtained under a H_2 pressure of 1 MPa (A); XRD patterns of raw material (Mg) are shown for comparison.

Fig. 7 − SEM images of the silver-gray material separated from the as-deposited product obtained at a H_2 pressure of 1 MPa. The above material was evaluated to be pure Mg by XRD as shown in Figure 6, the three right images are the higher magnification ones of the left three.

Fig. 8 − SEM images of the as-deposited MgH_2 products prepared at different H_2 pressures of 1 MPa (A), 2 MPa (B), 3 MPa (C) and 4 MPa (D). Insets show the higher magnification ones.

Fig. 9 − Typical morphology of the as-deposited products synthesized at different H_2 pressures, as well as the relationship between the production rate and H_2 pressure. Note that with increasing hydrogen pressure, the nanofibers change to a more straight, thin shape with a larger production rate. The one end of the 1MPa product (see arrow) was pure magnesium, magnesium hydride, due to the higher temperature in the chamber away from the substrate.

Fig. 1

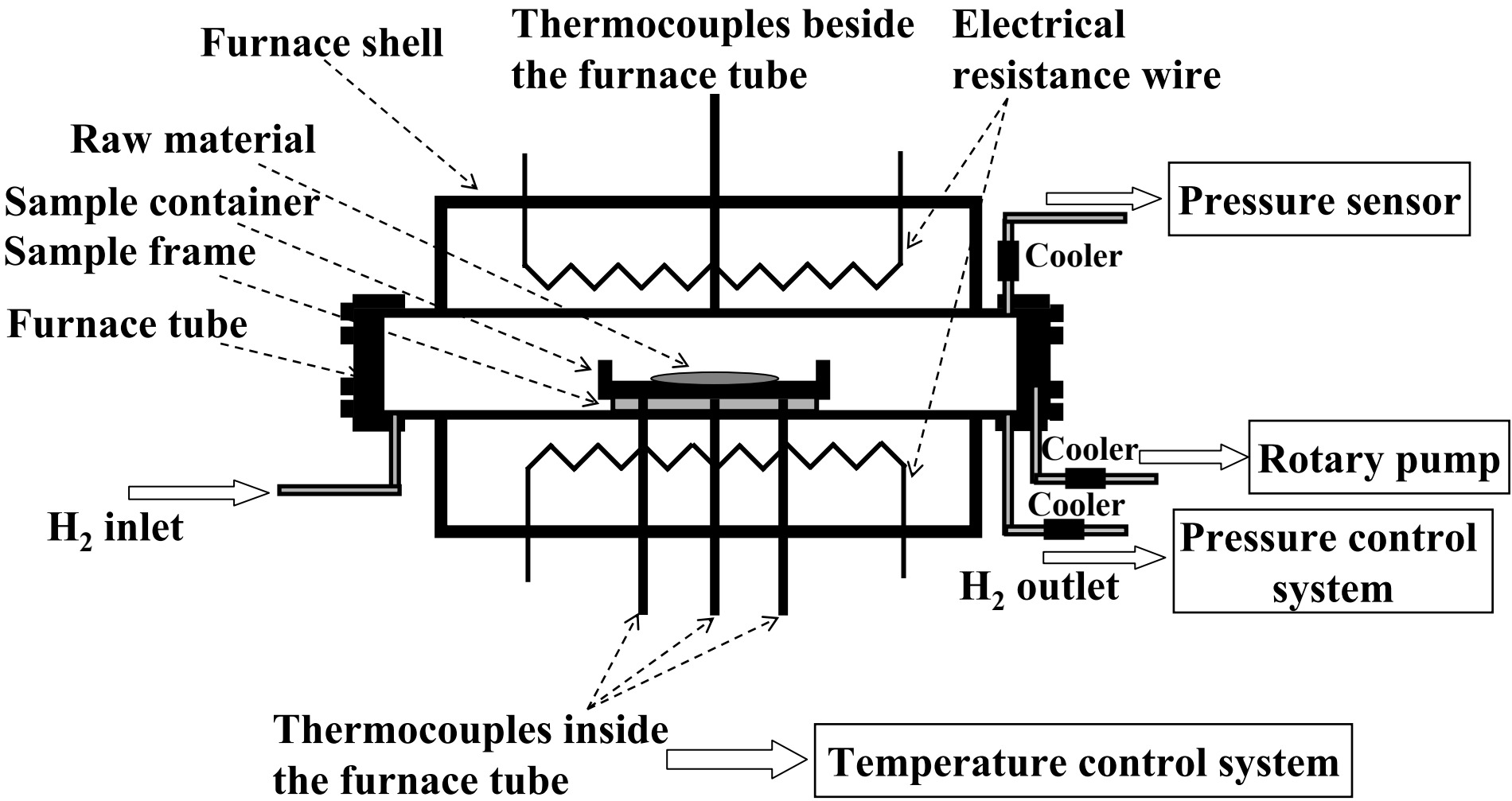
Furnace shell
Thermocouples beside the furnace tube
Electrical resistance wire
Raw material
Sample container
Sample frame
Furnace tube
Pressure sensor
Cooler
Cooler
Rotary pump
Cooler
Pressure control system
H2 inlet
H2 outlet
Thermocouples inside the furnace tube
Temperature control system

Fig. 2

(a)

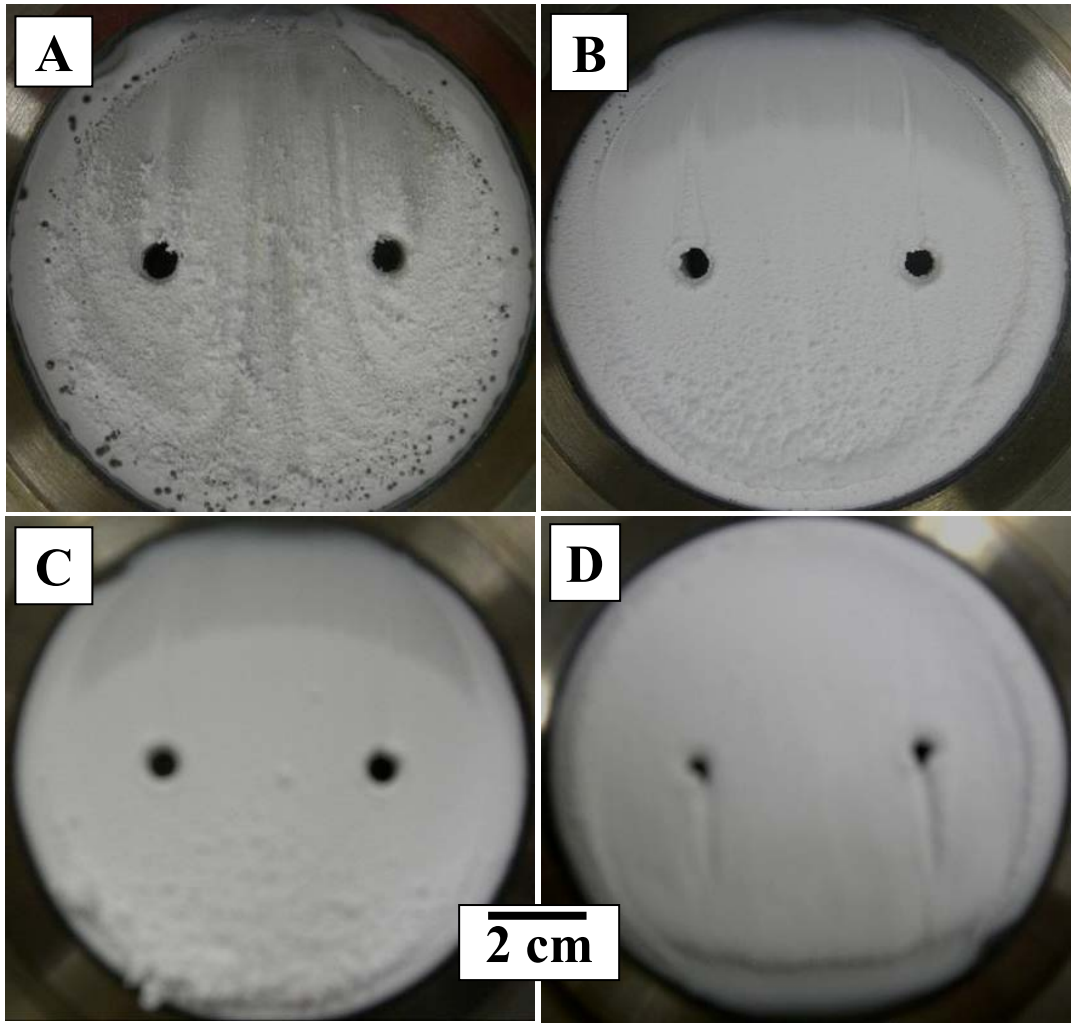

(b)

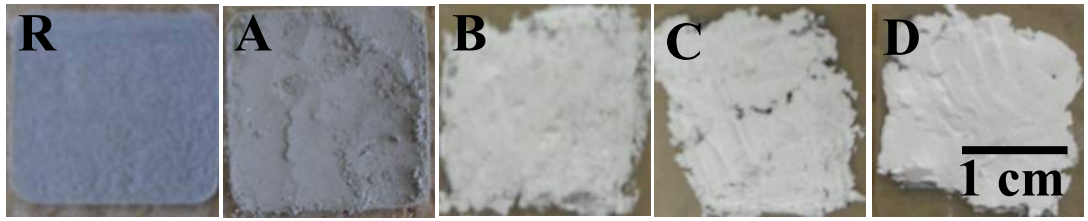

Fig. 3

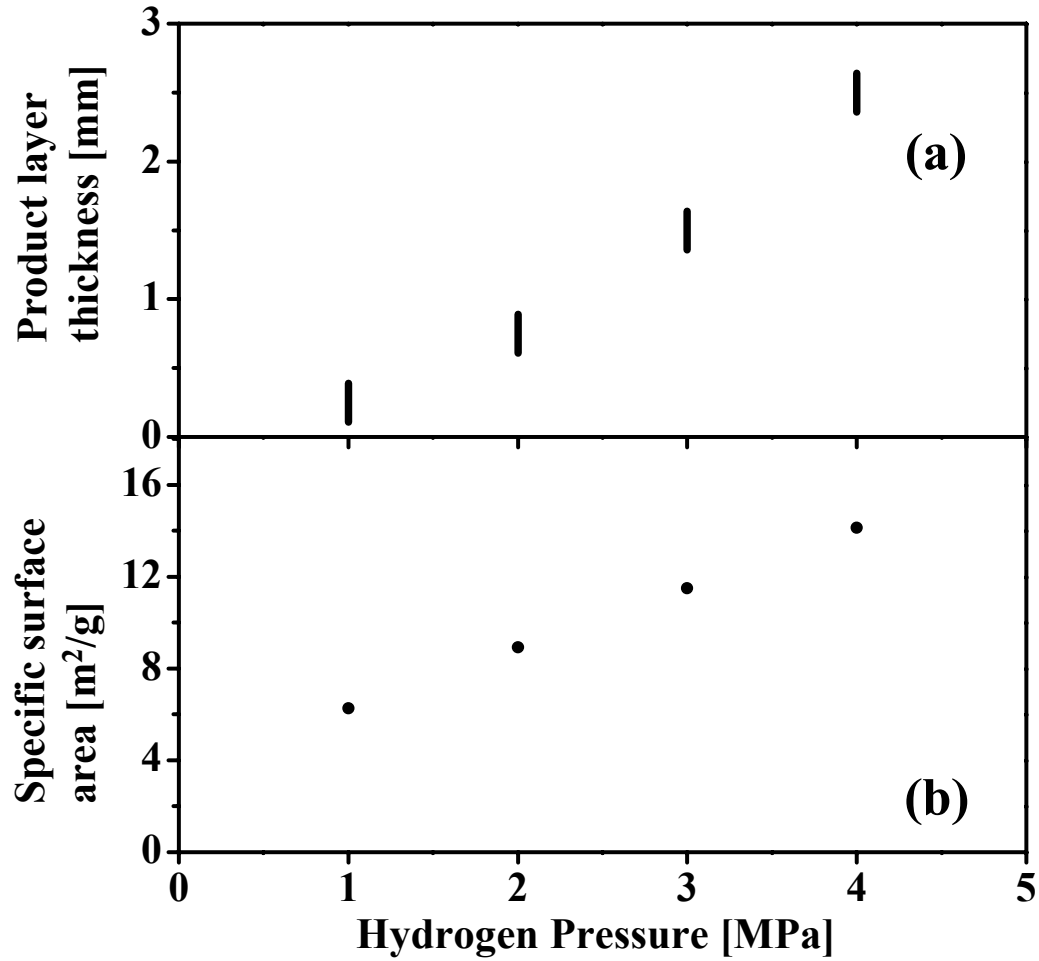
Product layer thickness [mm]
3
2
1
0
(a)
Specific surface area [m²/g]
16
12
8
4
0
(b)
0
1
2
3
4
5
Hydrogen Pressure [MPa]

Fig. 4

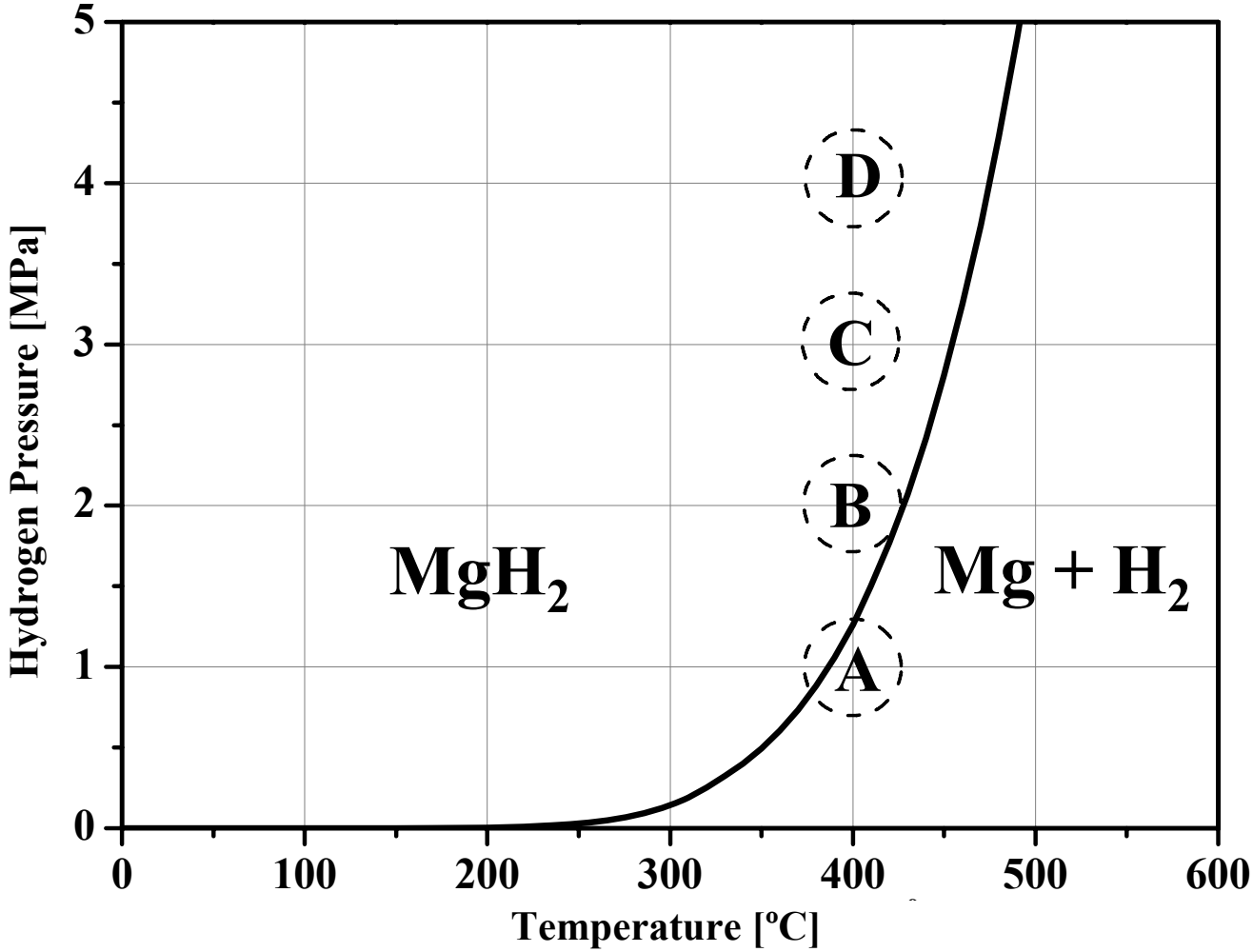
Hydrogen Pressure [MPa]
Temperature [ºC]
0
1
2
3
4
5
0
100
200
300
400
500
600
D
C
B
A
MgH2
Mg + H2

Fig. 5

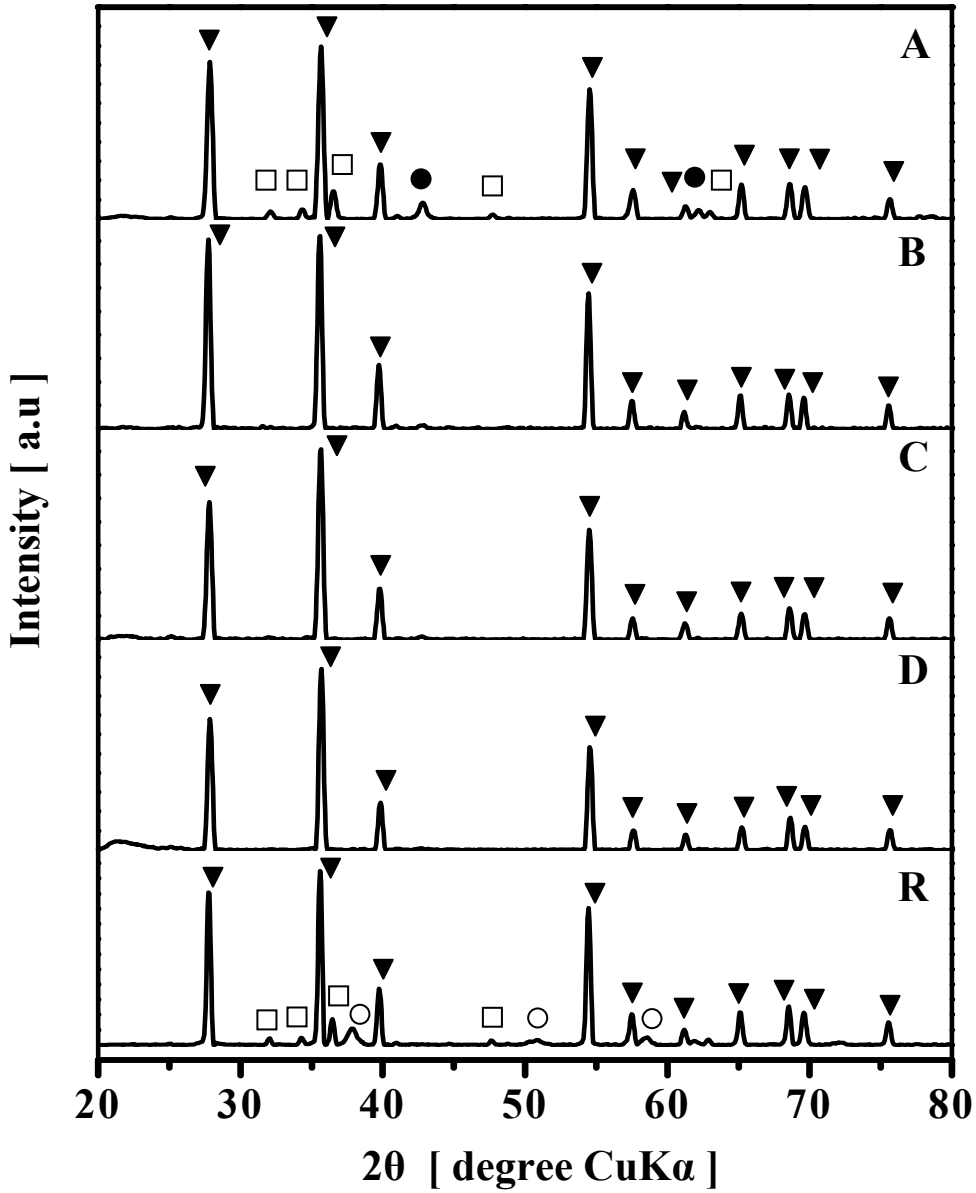

Fig. 6

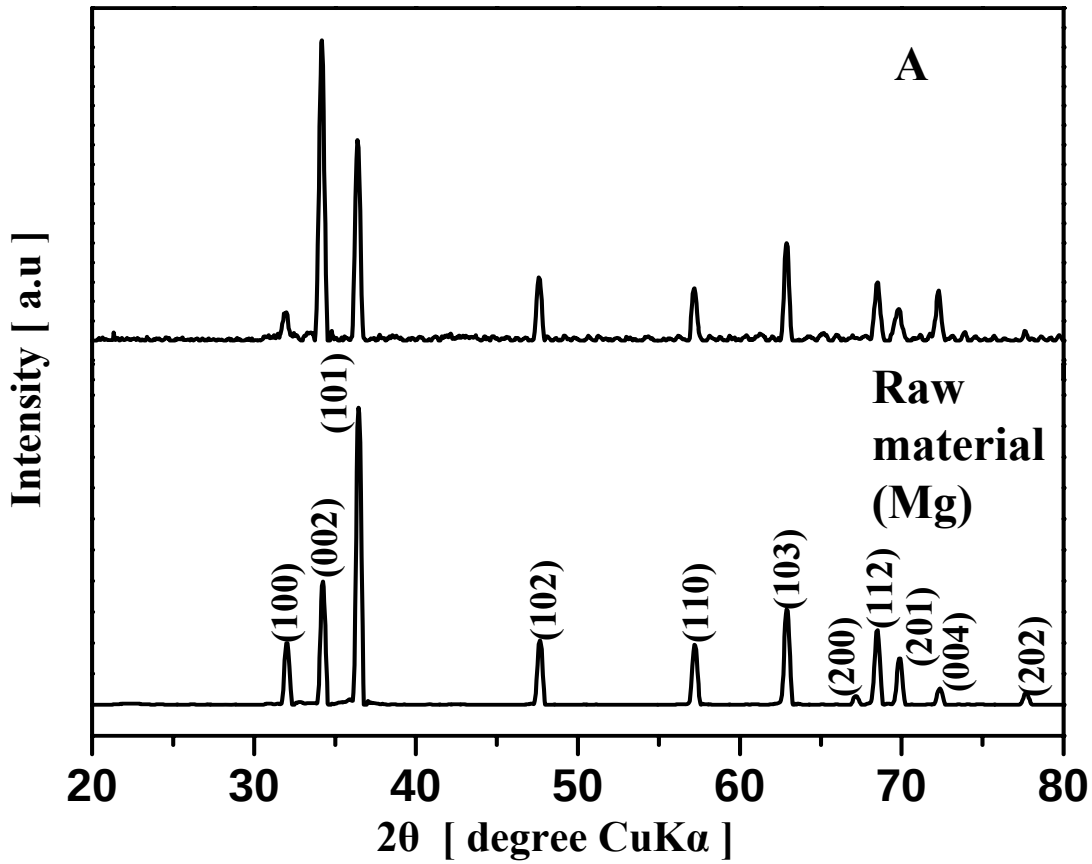
A
Raw material (Mg)
Intensity [a.u]
(100)
(002)
(101)
(102)
(110)
(103)
(200)
(112)
(201)
(004)
(202)
20
30
40
50
60
70
80
2θ [degree CuKα]

Fig. 7

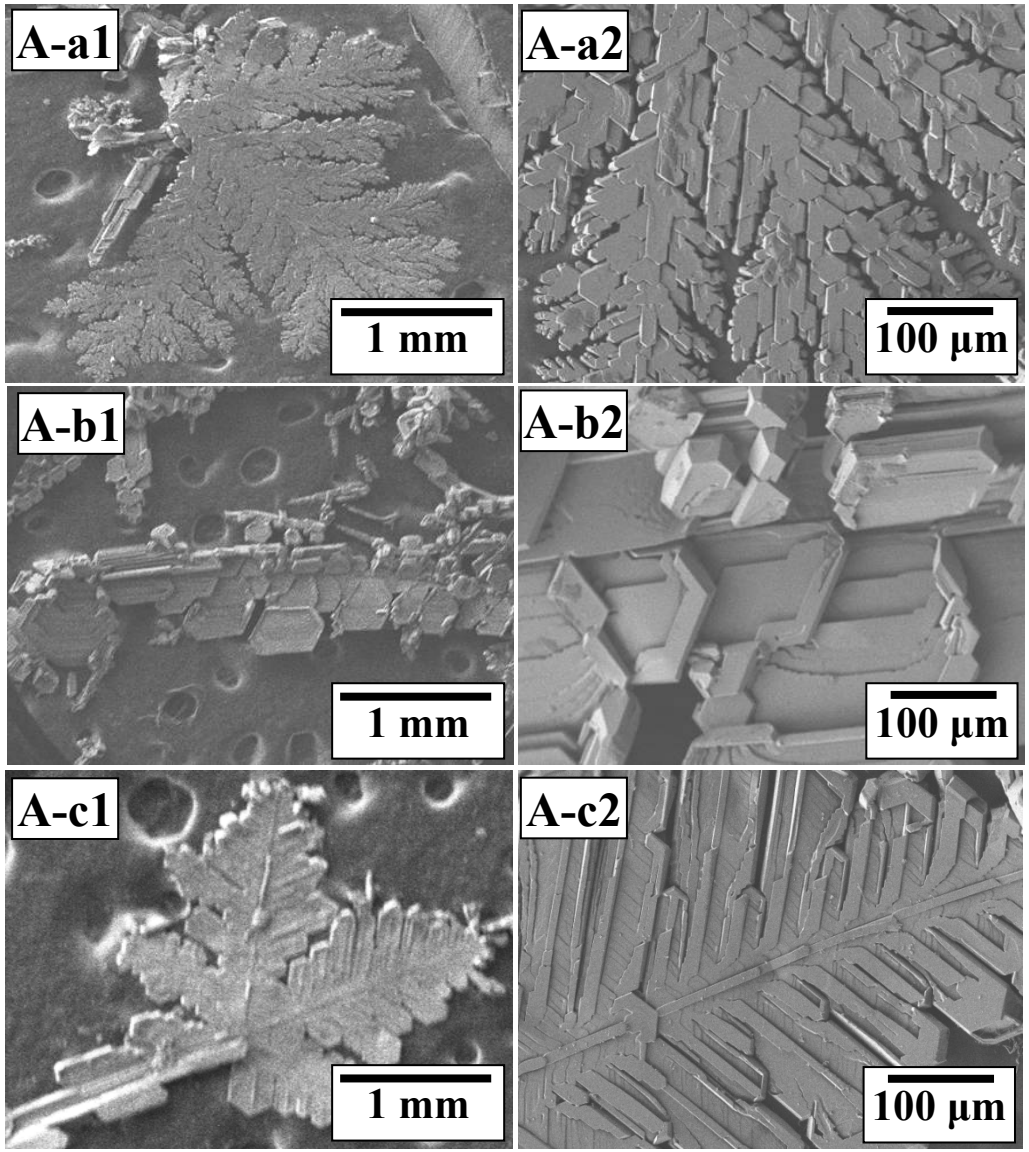

Fig. 8

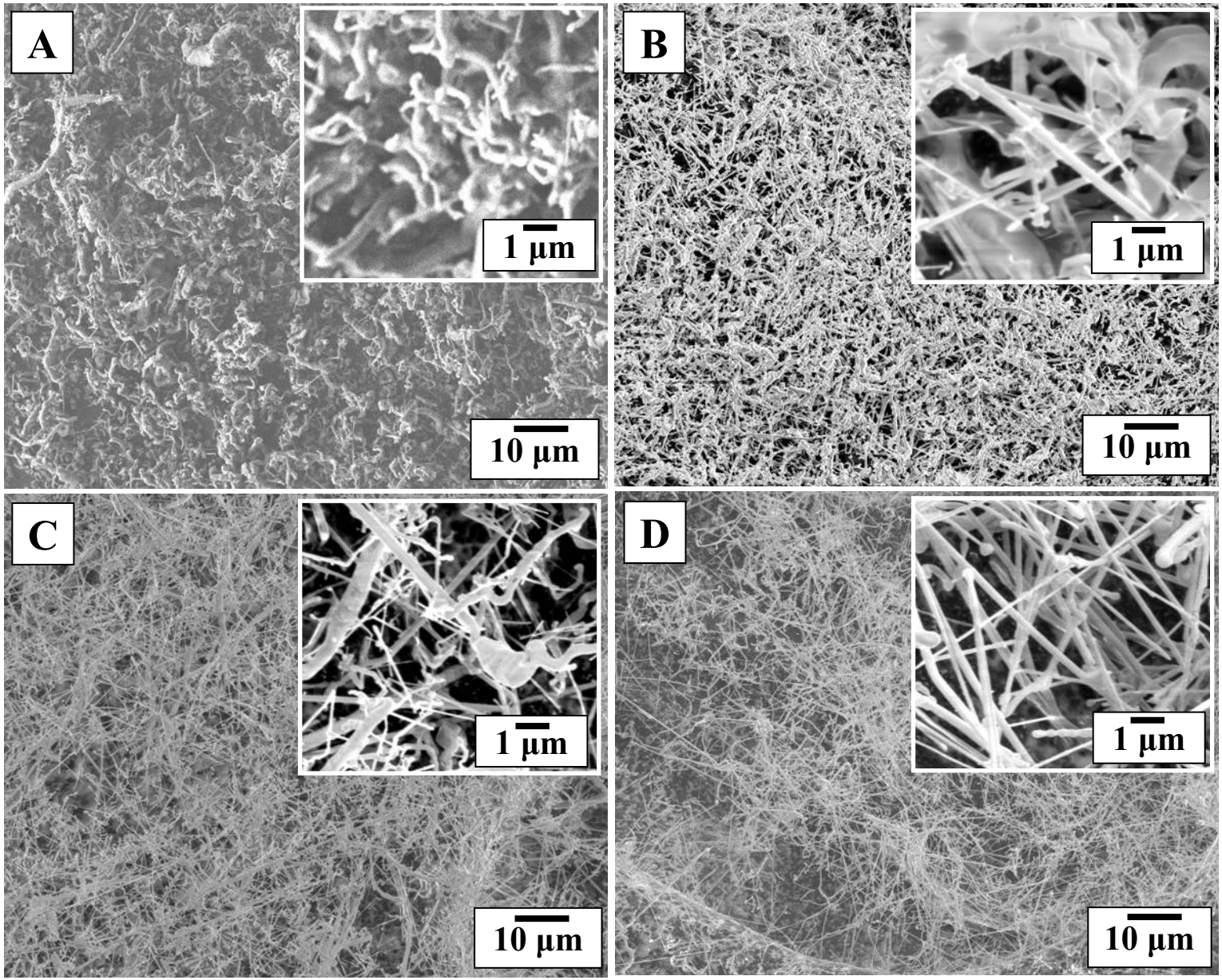

Fig. 9

P_{H_2}	*Morphology*[1]	*Shape*	*Diameter*	*Production Rate*
1 MPa				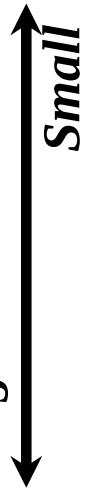
2 MPa	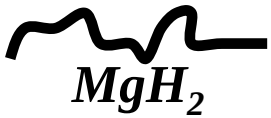			
3 MPa	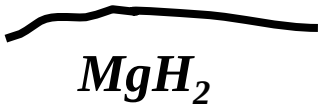			
4 MPa	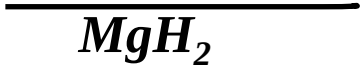			

[1]; Growth direction is ⟶